Stochastic Response Analysis, Order Reduction, and Output Feedback Controllers for Flexible Spacecraft

Hari B. Hablani*
Rockwell International, Seal Beach, California

Real disturbances and real sensors have finite bandwidths. The first objective of this paper is to incorporate this finiteness in the "open-loop modal cost analysis" as applied to a flexible spacecraft. Analysis based on residue calculus shows that among other factors, significance of a mode depends on the power spectral density of disturbances and the response spectral density of sensors at the modal frequency. The second objective of this article is to compare performances of an optimal and a suboptimal output feedback controller, the latter based on "minimum error excitation" of Kosut. Both the performances are found to be nearly the same, leading us to favor the latter technique because it entails only linear computations. Our final objective is to detect an instability due to truncated modes by representing them as a multiplicative and an additive perturbation in a nominal transfer function. In an example problem we find that this procedure leads to a narrow range of permissible controller gains, and that it labels a wrong mode as a cause of instability. A free beam is used to illustrate the analysis in this work.

I. Introduction

THE objectives of this paper are: a) to broaden the "open-loop modal cost analysis" so as to embrace disturbances having arbitrary power spectral densities and sensors having general response spectral densities, b) to compare performances of an optimal and a suboptimal output feedback controller, the latter based on Kosut's "minimum error excitation" technique,[7] and c) to detect any instability due to truncated modes by representing them as an additive or a multiplicative perturbation in a nominal transfer function of a flexible spacecraft. The organization of the paper along with a brief review of the relevant literature is as follows.

Hughes and Skelton[1] have enunciated a methodology for order reduction of flexible spacecraft from several different viewpoints, some of which can be interwoven to form a criterion now widely known as "modal cost". While deducing the modal costs, Skelton and Hughes[2] used white noise to model any random disturbances acting on a spacecraft. However, since all real disturbances have finite bandwidths, in contrast to white noise which has an infinite bandwidth, it is helpful to model them explicitly as such. Efforts in this direction were initiated in Ref. 3 where a few *specific* power spectral densities were considered. However, results for an arbitrary spectral density were left as a speculation. Section II of this paper completes this effort by deriving modal costs not only for arbitrary disturbances but also for sensors having arbitrary response spectral density. The stated objective is accomplished by a frequency domain approach based on residue calculus.

To accomplish the remaining objectives, a flexible spacecraft is considered whose attitude motion about at least one axis is decoupled from the motion about the other two axes and from the translational motion. In Sec. III a state space model is prepared and a single-input, single-output problem of controlling the attitude by output feedback is posed. Real, finite bandwidth disturbances experienced by a spacecraft are simulated by a combination of exponentially correlated noise and a second-order stochastic process. The latter typifies the noise due to an actuator. The modes are selected according to the modal cost relations developed in Sec. II.

An attitude controller can be designed by any of the various existing techniques. We will briefly comment only on linear quadratic Gaussian (LQG) and optimal output feedback (OOFB) schemes. When performance specifications for a spacecraft are stringent, a compatible mathematical description requires a large number of state variables which may far exceed the number of sensors employed. In principle, a Kalman filter can be used to estimate an arbitrary number of state variables. Nonetheless, due to limited memory of flight computers and due to a general lack of system-independent global robustness properties of an LQG controller, an OOFB controller may prove to be more flightworthy than an LQG controller. In fact, Ashkenazi and Bryson[4] have shown that the OOFB controllers may be generally more robust than the LQG controllers. With this motivation an OOFB controller will be designed in Sec. III. See Pearson and Johnson[5] for recent interpretations of optimal output feedback in terms of state feedback. The gains of an OOFB controller are determined by iteratively solving nonlinear parametric optimization problems. Usually, convergence of an iterative algorithm is a serious obstacle in the determination of an OOFB gain. Lin et al.[6] suggest that the "minimum error excitation" (MEE) approach for suboptimal output feedback, originated by Kosut,[7] may serve as a good initial guess for the computation of OOFB gains. These ideas are successfully tested in Secs. III and V where performance of an MEE controller is compared with that of an OOFB; this is the objective (b) of the paper. For completeness we note a recent extension of the minimum error excitation technique by Hegg[8] to account for a case in which the number of sensors are more than the number of configuration variables in the reduced order model.

We now focus on the modes not considered while designing the OOFB controller in Sec. III—the objective (c) of this paper. In Sec. IV these truncated modes are modeled as a multiplicative perturbation in the transfer function corresponding to the controller of Sec. III. The robustness criteria given by Doyle and Stein,[9] and Nuzman and Sandell[10] are invoked to check stability of the controller in the presence of the truncated modes. Kosut et al.[11] have adapted the robustness inequalities of Refs. 9 and 10 for flexible spacecraft and have illustrated them on the tetrahedral truss structure of the Charles Stark Draper Laboratory. It is known that the in-

Received July 26, 1982; presented as Paper 82-1613 at the AIAA Guidance and Control Conference, San Diego, Calif., Aug. 9-11, 1982; revision received Jan. 20, 1984.

*Member of Technical Staff. This work was done while the author was a NASA-NRC Research Associate at Johnson Space Center, Houston, Texas.

equalities are conservative. However, in Ref. 11 attempts are not made to validate the existence of the instability predicted by the inequalities. This will be done in the present paper. Various numerical results corresponding to the analysis in Sec. II to Sec. IV are discussed in Sec. V. Several important findings of this paper are summarized in Sec. VI.

II. Open-Loop Modal Cost Analysis for General Disturbances

The open-loop modal cost analysis is essentially a study in weakly stationary, linear random vibrations of structures. This analysis can be performed in both the time and frequency domains. In the time domain the structure may be modeled as a first-order system in state space and it may be driven by white noise. The relationship between the excitation and the response is expressed in the form of a Liapunov equation which may be solved in the time domain. Skelton and Hughes[2] adopted this approach. It turns out that this approach imposes more analytical labor than does the frequency domain approach, which is based on the method of residues. Consequently, it is the latter technique which is adopted in this paper.

A central assumption underlying the analysis in this section is that energy dissipation due to material hysteresis, friction associated with the structure's joints, or to any other source can be accounted for by a linear viscous damping coefficient, ζ, which is close to, but not equal to, zero. The literature suggests that $\zeta \simeq 0.005$ may be appropriate. To be sure, structural dissipation is neither viscous nor linear, yet the linear viscous representation is conventional and is permitted here. For a more precise model and a more complete discussion the reader may review Hughes.[12] The second assumption in this analysis is that the cross-correlation between two different modes is insignificant. Validity of this assumption depends on an overlap ratio r defined by (see Crandall and Wittig, Ref. 13).

$$r = \text{half power modal bandwidth/modal spacing}$$
$$= 2\zeta_m\omega_m/(\omega_m - \omega_{m-1}),\ m = 1, 2, \ldots, \infty \tag{1}$$

which must be $\ll 1$. In Eq. (1), ζ_m is the linear viscous damping coefficient of the mode m, and ω_m is its natural frequency. Unless specified otherwise $m = 1, 2, \ldots, \infty$, throughout the paper. Generally, for simple structures such as beams and strings, $r \ll 1$. However, r can be greater than unity for structures having tightly clustered frequencies. For example, for a certain shell structure the ratio r was found to be 5.984 for $m = 2$, and 1.387 for $m = 3$ (Ref. 14). In such situations the following analysis will require modifications parallel to those in Ref. 14. The third assumption in this analysis is with regard to the zero-frequency rigid modes of a spacecraft. It is assumed that the cross-correlation between the rigid modes and any flexible vehicle mode m is zero. In the early phase of our work this cross-correlation was incorporated. However, subsequent numerical experience showed that due to the light damping assumption, that is, $\zeta_m \to 0$, the rigid-elastic cross-correlation is negligible as compared to the modal auto-correlation. Expressions of the modal costs are now derived.

Consider an inertially stabilized spacecraft whose dynamics is such that there is at least one axis about which the attitude motion is uncoupled from the motion about the other two axes, and from translational motion. Further, assume that this attitude motion is controlled by one torquer, say a reaction wheel, located anywhere on the spacecraft. If there exists more than one torquer, the following analysis can be modified by a simple insertion of a summation sign in the right side of Eq. (2). The temporal behavior of the mth elastic vehicle mode under these idealizations is given by

$$\ddot{\eta}_m + 2\zeta_m\omega_m\dot{\eta}_m + \omega_m^2\eta_m = w'_{ma}u_a(t) \tag{2}$$

where η_m is the modal coordinate of the mode m; w'_{ma} is the slope of the mode where the torque $u_a(t)$ acts; the dot on η_m indicates time differentiation. In this section the point torque $u_a(t)$ is a zero-mean, weakly stationary random torque having a power spectral density $P_a(\omega)$ at the frequency ω; subsequently, it will include control torque also. In the s plane, Eq. (2) appears as

$$\eta_m(s) = u_a(s)w'_{ma}/(s^2 + 2s\zeta_m\omega_m + \omega_m^2) \tag{3}$$

For convenience the argument s will be dropped whenever appropriate.

Our objective is to determine $\lim_{t\to\infty} E(\eta_m^2) \triangleq E(\eta_m^2)_\infty$ where E is an expectation operator. Recall that (Theorem 1.50, Ref. 15)

$$E(\eta_m^2)_\infty = \frac{1}{2\pi}\int_{-\infty}^{\infty} P_{\eta m}(\omega)\,\mathrm{d}\omega \tag{4}$$

where $P_{\eta m}(\omega)$ is the power spectral density of $\eta_m(t)$. Equation (4) is true because $\eta_m(t)$ is a wide-sense stationary stochastic process with zero mean. To evaluate $P_{\eta m}(\omega)$ we apply Theorem 1.49 of Ref. 15 to Eq. (3) which leads to

$$P_{\eta m}(\omega) = P_a(\omega)w'^2_{ma}/\{(-\omega^2 + \omega_m^2) + 2j\zeta_m\omega_m\omega\}$$
$$\{(-\omega^2 + \omega_m^2) - 2j\zeta_m\omega_m\omega\} \tag{5}$$

where $j^2 = -1$. Equation (5) is now substituted in Eq. (4). For evaluating the improper integral in Eq. (4) we invoke the following theorem from Hildebrand[16]

$$\int_{-\infty}^{\infty} f(\omega)\,\mathrm{d}\omega = 2\pi j\sum_k \mathrm{Res}(a_k) \tag{6}$$

which is valid if the denominator of $f(\omega)$ is of degree at least two greater than the numerator. The points a_k are the poles of $f(z)$ in the upper half plane of z, and $\mathrm{Res}(a_k)$ is the residue of $f(z)$ at a_k. Here $f(z)$ is obtained from $f(\omega)$ by replacing ω^2 with z^2 where z is a complex variable. The poles and the residues are due to the mth vehicle mode and due to the power spectral density $P_a(z)$. The former set has the following four poles

$$z_{1,2} \simeq \pm\omega_m + j\zeta_m\omega_m,\quad z_{3,4} \simeq \pm\omega_m - j\zeta_m\omega_m \tag{7}$$

The poles $z_{1,2}$ in Eq. (7) are in the upper half plane of z, and, therefore, $a_{1,2} \triangleq z_{1,2}$. On the other hand, the poles $z_{3,4}$ are in the lower half plane of z and, hence, are to be ignored. It can be proved that[16]

$$\mathrm{Res}(a_1) = P_a(a_1)/8j\zeta_m\omega_m^3(1 + j\zeta_m),$$
$$\mathrm{Res}(a_2) = P_a(a_2)/8j\zeta_m\omega_m^3(1 - j\zeta_m) \tag{8}$$

Due to the assumption that $\zeta_m \to 0$, $\mathrm{Res}(a_1)$ and $\mathrm{Res}(a_2)$ given by Eq. (8) dominate the remaining residues in Eq. (6) where the remaining residues are due to the power spectral density $P_a(z)$. Consequently, the sum in the right side of Eq. (6) can be approximated as follows

$$\int_{-\infty}^{\infty} f(\omega)\,\mathrm{d}\omega \simeq 2\pi j[\mathrm{Res}(a_1) + \mathrm{Res}(a_2)] \tag{9}$$

Setting Eq. (8) in Eq. (9) and recognizing that

$$P_a(\omega_m) = P_a(-\omega_m),\quad P_a(a_1) \simeq P_a(a_2) \simeq P_a(\omega_m) \tag{10}$$

Eq. (4) leads to

$$E(\eta_m^2)_\infty = w'^2_{ma}P_a(\omega_m)/4\zeta_m\omega_m^3 \tag{11}$$

which is the desired relationship. Equation (11) can be used for an internal disturbance caused by an actuator having a finite bandwidth.

In order to establish some guidelines about the range of validity of Eq. (11) we sacrifice generality for a moment and deal with specific disturbance models. A white noise disturbance, which does not introduce any poles in $P_{\eta m}(\omega)$ in Eq. (5), will give Eq. (11) rigorously, with $P_a(\omega_m)$ replaced by the constant power spectral density of the white noise. Indeed, for a spring mass system subject to white noise excitation a relationship similar to Eq. (11) is recorded in Bendat and Piersol[17] [see its Eq. (5.59)] where it is stated that such relationships are fairly accurate if $P_a(\omega)$ remains constant in the range $(1-6\zeta_m)\omega_m < \omega < (1+6\zeta_m)\omega_m$. We will also consider an exponentially correlated disturbance, which is used often to represent gyro noise and other statistical phenomena. Mathematically, an exponentially correlated stimulus $e(t)$ is modeled as

$$\dot{e} + e/\tau = \nu_e(t), \quad \nu_e \triangleq \mathcal{N}(0, V_e) \tag{12}$$

where τ is the time constant of $e(t)$ and $\nu_e(t)$ is the white noise of intensity V_e. Let σ_e^2 be the variance of $e(0)$; then $V_e = 2\sigma_e^2/\tau$. The power spectral density $P_e(\omega)$ of $e(t)$ is given by

$$P_e(\omega) = V_e/(\omega^2 + 1/\tau^2). \tag{13}$$

When $P_e(\omega)$ replaces $P_a(\omega)$ in Eq. (5), two poles, $z_{5,6} = \pm j/\tau$, in addition to those in Eq. (7), come to be recognized. Out of these two poles, incorporating the residue of $z_5 = +j/\tau$ in Eq. (9) and utilizing the assumption $\zeta_m \to 0$ it can be shown that

$$E(\eta_m^2)_\infty = w_{ma}'^2 P_e(\omega_m)/4\zeta_m\omega_m^3 + w_{ma}'^2\sigma_e^2/(\omega_m^2 + 1/\tau^2)^2 \tag{14}$$

On comparing Eq. (14) with Eq. (11) we notice the presence of an additional term in Eq. (14). The first term is the mean square vibration amplitude which would have been excited if the mode m were subjected to the white noise of intensity $P_e(\omega_m)$. This term represents the vibration of the mode m in its resonance range and consequently is inversely proportional to the modal damping ζ_m. The second term, on the other hand, represents the excitation of the mode m due to the power spectrum of $e(t)$ outside the half-power modal bandwidth $2\zeta_m\omega_m$. This term originates from the characteristic frequency $1/\tau$ at which the power of the disturbance $e(t)$ decreases drastically. Generally, the second term seems to be less significant than the first because the first term is inversely proportional to ζ_m, which is close to zero and to ω_m^3, whereas the second term is inversely proportional to ω_m^4. Consequently, the following approximation of Eq. (14) is *generally* correct

$$E(\eta_m^2)_\infty = w_{ma}'^2 P_e(\omega_m)/4\zeta_m\omega_m^3 \tag{15}$$

which is a special case of Eq. (11). However, consider a constant disturbance which can be modeled by Eq. (12) by letting $1/\tau = 0$, $V_e = 0$ and, therefore, $P_e(\omega) = 0$ for $\omega \neq 0$. Equation (14) then reduces to

$$E(\eta_m^2)_\infty = w_{ma}'^2\sigma_e^2/\omega_m^4 \tag{16}$$

where now, $\sigma_e \triangleq e(0)$. That Eq. (16) is correct can be verified by realizing that for a constant disturbance

$$\dot{\eta}_m(\infty) = 0, \qquad \ddot{\eta}_m(\infty) = 0 \tag{17}$$

for all elastic modes (not for a zero-frequency rigid mode). Putting Eq. (17) in Eq. (2) and recalling that $u_a(t)$ is now a constant disturbance σ_e, Eq. (16) is recovered. Note that the constant torque σ_e has the power σ_e^2 which appears in Eq. (16) and its power spectral density equals $P_e(\omega) = 2\pi\sigma_0^2 U_0(\omega)$, where $U_0(\omega)$ is the Dirac delta function with a unit area.

The engineer who is interested in the stochastic vibrations due to exponential disturbances correlated not only in time, as in the preceding, but also in space, may refer to the book by Skudrzyk.[18]

We now turn our attention to the evaluation of $E(\dot{\eta}_m^2)_\infty$. Clearly

$$E(\dot{\eta}_m^2)_\infty = \frac{1}{2\pi}\int_{-\infty}^{\infty} \omega^2 P_{\eta m}(\omega)\,\mathrm{d}\omega \tag{18}$$

where $P_{\eta m}(\omega)$ is given by Eq. (5). The factor ω^2 does not introduce any additional poles. Consequently, retracing the path followed from Eq. (2) to Eq. (11) under the same assumptions, we can prove that

$$E(\dot{\eta}_m^2)_\infty = w_{ma}'^2 P_a(\omega_m)/4\zeta_m\omega_m \tag{19}$$

Again, a relationship more rigorous than Eq. (19) can be given for the exponentially correlated disturbance $e(t)$. It is

$$E(\dot{\eta}_m^2)_\infty = w_{ma}'^2 P_e(\omega_m)/4\zeta_m\omega_m - w_{ma}'^2\sigma_e^2/\left\{\tau^2(\omega_m^2 + 1/\tau^2)^2\right\} \tag{20}$$

Comparing Eq. (20) with Eq. (14) we learn that the relationship

$$E(\dot{\eta}_n^2)_\infty = \omega_m^2 E(\eta_m^2)_\infty \tag{21}$$

is *not always* true. Only the first terms in Eq. (14) and Eq. (20) are related according to Eq. (21), whereas the second term in Eq. (20) is $(-1/\tau^2)$ times the second term in Eq. (14). Yet the mean square modal velocity in the resonance region, the first term in Eq. (20), usually predominates, and in practice, both Eq. (19) and Eq. (21) are correct. Also, it is encouraging to note that for a constant disturbance, that is, $1/\tau = 0$ and $P_e(\omega) = 0$ for $\omega \neq 0$, Eq. (20) agrees with the first equation in Eqs. (17) which were written intuitively.

We will now study the influence of sensor dynamics on $E(\eta_m^2)_\infty$ in Eq. (11). Attitude sensors typically include gyroscopes, horizon sensors, and star trackers. Sensors vary widely in the accuracy and in the physical principles underlying the estimates of attitude and attitude rates (Ref. 19). Figure 1 shows the block diagram of the mode m being excited by an actuator having the transfer function $g_a(s)$ and being sensed by a sensor having the transfer function $g_s(s)$. Clearly,

$$u_a(s) = g_a(s)u(s), \quad \eta_m(s) = h_m(s)u_a(s), \quad \hat{\eta}_m = g_s(s)\eta_m \tag{22}$$

where the definition of $h_m(s)$ is evident from Eq. (3). It is helpful to combine the actuator and the sensor transfer functions by defining a quantity u_a' thus

$$u_a'(s) \triangleq g_s(s)g_a(s)u(s) \tag{23}$$

With the aid of Eq. (23) the sensor output $\hat{\eta}_m(s)$ in Eq. (22)

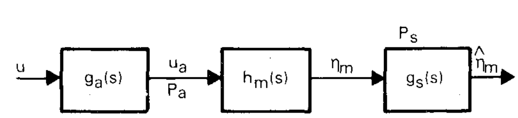

Fig. 1 Modal excitation as sensed by a real sensor.

can be cast as

$$\hat{\eta}_m(s) = h_m(s)\,u_a'(s) \tag{24}$$

By comparing Eq. (24) with the second equation in Eqs. (22) we observe that $E(\hat{\eta}_m^2)_\infty$ can be obtained from $E(\eta_m^2)_\infty$ by replacing the power spectral density $P_a(\omega)$ of u_a in Eq. (11) with the spectral density $P_a'(\omega)$ of u_a'. From the definition, Eq. (23), and the first equation of Eqs. (22), there follows

$$P_a'(\omega) = g_s(-j\omega)\,P_a(\omega)\,g_s(j\omega) \tag{25}$$

If the response spectral density $P_s(\omega)$ of a sensor is defined by

$$P_s(\omega) \triangleq g_s(-j\omega)\,g_s(j\omega), \tag{26}$$

then

$$P_a'(\omega) = P_a(\omega)\,P_s(\omega) \tag{27}$$

Thus, from Eq. (11) it follows that

$$E(\hat{\eta}_m^2)_\infty = w_{ma}'^2 P_a(\omega_m)\,P_s(\omega_m)/4\zeta_m\omega_m^3 \tag{28}$$

Similarly, Eq. (19) yields

$$E(\hat{\dot{\eta}}_m^2)_\infty = w_{ma}'^2 P_a(\omega_m)\,P_s^r(\omega_m)/4\zeta_m\omega_m \tag{29}$$

where $P_s^r(\omega_m)$ is the response spectral density of a rate sensor.

We recognize that a single modal coordinate $\eta_m(t)$ cannot be sensed, contrary to what is portrayed in Fig. 1; it is always the total attitude $\theta(t)$ or the rate $\dot{\theta}(t)$ which are sensed. Under the conditions stated in the paragraph before Eq. (2) the small angular motion $\theta(t)$ of a spacecraft can be expressed as

$$\theta(t) = \eta_0(t) + \sum w_{ms}'\eta_m(t), \quad \sum \triangleq \sum_{m=1}^{\infty} \tag{30}$$

where w_{ms}' is the slope of the mth vehicle mode at the location where attitude is of interest. The variable $\eta_0(t)$ in Eq. (30) is a zero-frequency rigid mode. If

$$\theta_m(t) \triangleq w_{ms}'\eta_m(t), \quad \dot{\theta}_m(t) \triangleq w_{ms}'\dot{\eta}_m(t), \tag{31}$$

with the aid of Eq. (11) and Eq. (19) we can see that

$$E(\theta_m^2)_\infty = w_{ma}'^2 w_{ms}'^2 P_a(\omega_m)/4\zeta_m\omega_m^3 \tag{32}$$

$$E(\dot{\theta}_m^2)_\infty = w_{ma}'^2 w_{ms}'^2 P_a(\omega_m)/4\zeta_m\omega_m \tag{33}$$

Similarly, if the sensor output is defined as

$$\hat{\theta}_m(t) \triangleq w_{ms}'\hat{\eta}_m(t), \quad \hat{\dot{\theta}}_m(t) \triangleq w_{ms}'\hat{\dot{\eta}}_m(t), \tag{34}$$

Eqs. (28), (29) lead to

$$E(\hat{\theta}_m^2)_\infty = w_{ma}'^2 w_{ms}'^2 P_a(\omega_m)\,P_s(\omega_m)/4\zeta_m\omega_m^3 \tag{35a}$$

$$E(\hat{\dot{\theta}}_m^2)_\infty = w_{ma}'^2 w_{ms}'^2 P_a(\omega_m)\,P_s^r(\omega_m)/4\zeta_m\omega_m \tag{35b}$$

For collocated actuators and sensors, note that $w_{ma}' = w_{ms}'$.

With the derivation of the four modal indices, $E(\eta_m^2)_\infty$, $E(\dot{\eta}_m^2)_\infty$, $E(\theta_m^2)_\infty$, and $E(\dot{\theta}_m^2)_\infty$, in Eqs. (11), (19), (32), and (33) under different circumstances, the objective (a) of this paper has been accomplished. The indices will be illustrated in Sec. V.

III. State Space Model for Output Feedback Controllers

The four modal indices developed in the previous section were derived to construct a reduced-order model of a spacecraft. A reduced-order model is required to accomplish our next objective, comparison of the performance of an optimal output feedback with that of a "minimum error excitation" suboptimal output feedback. We now address ourselves to this objective.

We wish to pose an output feedback problem which is at once typical, yet simple. The simple control block diagrams shown in Fig. 2 meet these criteria (the perturbation blocks $1+L(s)$ and $G_H(s)$ will be discussed in the next section). As shown in Fig. 2 our objective is to control the attitude $\theta(t)$ of the spacecraft under analysis. Recalling Eq. (30) we observe that the zero-frequency rigid mode η_0 is unstable, neither is it stabilizable by the posed single-input, single-output problem because of the unavailability of the attitude rate $\dot{\theta}(t)$. Before any study on optimal or suboptimal output feedback can be initiated, it is necessary to eliminate this instability. Since it is not within the intended scope of this paper to design a controller to achieve desired location of the rigid-body poles, we will simply replace the unstable rigid mode

$$C\ddot{\eta}_0 = e(t) + u_a(t) \tag{36}$$

with the following well damped mode having the frequency $\omega_0 = 0.26413 \times 10^{-3}$ rad/s and the damping coefficient $\zeta_0 = 0.70888$ (these numbers were provided by an optimal state feedback study):

$$C(\ddot{\eta}_0 + 2\zeta_0\omega_0\dot{\eta}_0 + \omega_0^2\eta_0) = e(t) + u_a(t) \tag{37}$$

where C is the moment of inertia of the spacecraft about the axis of the rotation $\theta(t)$. Some comments about how realistic this replacement is are desired. The frequency ω_0 and the damping coefficient ζ_0 might be introduced by the "classical" proportional plus derivative controller. However, the sensor, a rate gyro for instance, and the actuator, say, a thruster, will have to have a narrow bandwidth so that the elastic modes are left unobserved and unexcited. If this is practical, then a mathematical model of such a sensor and an actuator should be appended to Eq. (37). This, however, is not done here and the question whether the above replacement is realistic will not be pursued further.

Returning to our objective of comparing two output feedback schemes, we now have the following dynamics to consider:

rigid mode:

$$C(\ddot{\eta}_0 + 2\zeta_0\omega_0\dot{\eta}_0 + \omega_0^2\eta_0) = e(t) + u_a(t) \tag{38a}$$

elastic modes:

$$\ddot{\eta}_m + 2\zeta_m\omega_m\dot{\eta}_m + \omega_m^2\eta_m = w_{ma}'(e+u_a), \quad m = m_1,\ldots,m_N; \tag{38b}$$

disturbance:

$$\dot{e} + e/\tau = v_e(t), \quad v_e \triangleq \mathcal{N}(0,V_e) \tag{38c}$$

actuator dynamics:

$$\ddot{u}_a + 2\zeta_a\omega_a\dot{u}_a + \omega_a^2 u_a = \omega_a^2(u+v_a), \quad v_a \triangleq \mathcal{N}(0,V_a) \tag{38d}$$

In writing Eqs. (38) the sensor dynamics has been ignored for convenience. Later it will be assumed that the sensor and the actuator are collocated. In addition to the rigid mode controller described above, we introduce an output feedback

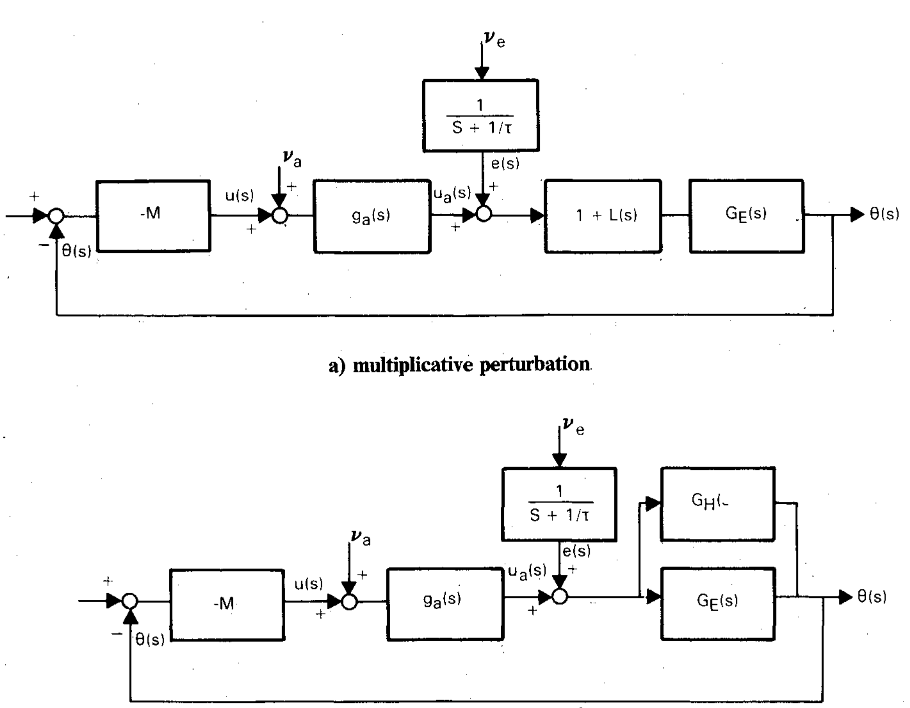

a) multiplicative perturbation

b) additive perturbation

Fig. 2 Truncated modes as a perturbation in idealized transfer function.

controller exerting the torque $u_a(t)$ at the location where attitude is to be controlled. The rigid mode controller may be regarded as a coarse attitude controller functioning implicitly in an inner loop, while the output feedback controller is thought to provide a fine supplementary attitude control of the spacecraft working in an outer loop. The elastic modes

$$m_1, m_2, \ldots, m_N, \tag{39}$$

where N = number of modes retained, are included in the model, Eq. (38). Selection of these modes will be discussed shortly. As shown in Fig. 2, $u(t)$ in Eq. (38d) is the control variable and is related to the output $\theta(t)$ thus

$$u(t) = M\theta(t) \tag{40}$$

where M is a negative scalar controller gain. The evaluation of M will be discussed in a moment. The actuator is modeled to furnish the control torque $u(t)$ as well as an undesirable internal disturbance originating from the white noise $\nu_a(t)$ which is filtered by a second-order dynamics of the actuator. $e(t)$ is the external disturbance explained already in Sec. II. It is straightforward to arrange Eqs. (38) in the following standard state space form

$$\dot{x}(t) = Ax(t) + bu(t) + b\nu_a(t) + \gamma\nu_e(t), \theta(t) = cx(t) \tag{41}$$

To conserve space, the detailed definitions of various notations in Eq. (41) will not be given here. They may, however, be reviewed in Ref. 20.

Regarding the modes to be retained, since our objective is to control the attitude $\theta(t)$ we can select those modes which have high $E(\theta_m^2)_\infty$ as given by Eq. (32) where now $P_a(\omega_m)$ will cover all the disturbances—$e(t)$ and $\nu_a(t)$—with the latter being filtered by Eq. (38d). For the purpose of illustration, however, we will compose a general control objective such as

$$J \triangleq \lim_{t \to \infty} E\Big[\theta^2(t) + \beta\dot{\theta}^2(t) + \gamma \sum \{\dot{\eta}_m^2(t) + \omega_m^2\eta_m^2(t)\} + \rho u^2(t)\Big] \tag{42}$$

which includes attitude, attitude rate, deformational kinetic and strain energies, and the control energy. β, γ, and ρ in Eq. (42) are weighting scalars. Initially, the summation sign in Eq. (42) includes, theoretically, an infinite number of modes.

On the basis of the assumption of zero cross-correlation among the modes discussed in Sec. II, the index J can be written as (ignore the rigid mode and the control energy temporarily)

$$J = \sum J_m, J_m \triangleq E\big[\theta_m^2 + \beta\dot{\theta}_m^2 + \gamma(\dot{\eta}_m^2 + \omega_m^2\eta_m^2)\big]_\infty \tag{43}$$

where θ_m and $\dot{\theta}_m$ are defined in Eq. (31). When the weighting scalars β and γ, disturbances, characteristics of actuators and sensors are specified, the index J_m in Eq. (43) can be evaluated by determining the modal indices of Sec. II. A sequence of modes, $m_1, m_2, \ldots, m_\infty$, can then be formed such that $J_{m1} > J_{m2} > \cdots > J_{m\infty}$, and as many modes may be retained as desired. After selecting appropriate modes the finite state space model can be readily constructed.

The controller gain M will first be determined by the "minimum error excitation" technique formulated by Kosut.[7] His formulation is based on nonzero initial conditions, and is slightly modified here to include disturbances. This formulation is linear and the scalar gain M is computed after determining a full state feedback controller for the model Eqs. (40)–(42). Using this as an initial guess the optimal output feedback gain M can be computed iteratively by solving the nonlinear optimization problem associated with the model. This nonlinear formulation is explained in Ref. 5. Since the mathematical details of the two techniques are standard and have been recorded in the conference paper (Ref. 20), they will not be repeated here. A comparison between the two output feedback schemes will be illustrated in Sec. V.

IV. Truncated Modes: Their Characterization and Influence

Our final objective is to determine if the modes which were truncated in Sec. III cause any instability in the presence of the output feedback controller. For this purpose, the deleted modes will be treated as an additive or a multiplicative perturbation in the idealized transfer function of the spacecraft.

In the absence of any external or internal disturbances and of any actuator/sensor characteristics, the following relationship between the attitude $\theta(s)$ and the control torque $u(s)$ can be easily shown

$$\theta(s) = G(s)u(s),$$
$$G(s) = 1/C(s^2 + 2\zeta_0\omega_0 s + \omega_0^2) + \sum g_m(s) \qquad (44)$$

where for a collocated pair of actuator and sensor

$$g_m(s) \triangleq w_{ma}'^2/(s^2 + 2s\zeta_m\omega_m + \omega_m^2) \qquad (45)$$

If retaining the modes $m_1, m_2, \ldots, m_N$ is thought to be appropriate, $G(s)$ in Eq. (44) can be partitioned as

$$G(s) = G_E(s) + G_H(s) \qquad (46a)$$

where

$$G_E(s) = 1/C(s^2 + 2\zeta_0\omega_0 s + \omega_0^2) + \sum_{m=m_1}^{m=m_N} g_m(s),$$
$$G_H(s) = \sum_{m=m_{N+1}}^{\infty} g_m(s) \qquad (46b)$$

We regard G_E as the nominal transfer function of the spacecraft and G_H as an additive perturbation to it. To express $G_H(s)$ as a multiplicative perturbation, Eq. (46a) can be arranged as

$$G(s) = [1 + L(s)]G_E(s), L(s) = G_H(s)G_E^{-1}(s) \qquad (47)$$

where $L(s)$ is a multiplicative perturbation in $G_E(s)$.

The above representation of the truncated modes in the form of a perturbation is for a single-loop system. A similar development for a multi-loop system can be seen in Refs. 3 and 11. Let us now re-insert the external and internal disturbances and the actuator characteristics into our discussion. The block diagrams corresponding to the state space model, Eq. (41), in conjunction with the truncated modes modeled according to Eqs. (46) and (47), are shown in Figs. 2a and 2b, where

$$g_a(s) = \omega_a^2/(s^2 + 2s\zeta_a\omega_a + \omega_a^2), e(s) = \nu_e/(s + 1/\tau).$$

The transfer function $g_a(s)$ is associated with the actuator described by Eq. (38d). From these diagrams, clearly

$$\text{M.P.:} \quad \theta(s) = g_a(1+L)G_E u + g_a(1+L)G_E\nu_a + (1+L)G_E e \qquad (48a)$$

$$\text{A.P.:} \quad \theta(s) = g_a(G_E + G_H)u + g_a(G_E + G_H)\nu_a + (G_E + G_H)e \qquad (48b)$$

where M.P. means multiplicative perturbation and A.P. means additive perturbation.

With these preliminaries we can now apply the robustness inequalities of Refs. 9 and 10 to the block diagrams in Fig. 2. There follows

$$\text{M.P.:} \quad |G_H G_E^{-1}| < |1 - (Mg_a G_E)^{-1}|, \qquad 0 \le \omega \le \infty \qquad (49a)$$

$$\text{A.P.:} \quad |Mg_a G_H| < |1 - Mg_a G_E|, \qquad 0 \le \omega \le \infty \qquad (49b)$$

where, we recall, M is a negative gain.

V. Numerical Results and Discussion

Illustration of the preceding analysis requires a numerical model of a flexible spacecraft. To reduce the level of unnecessary structural details without any loss in understanding, we select a free beam of length 2ℓ representing one class of future large space structures. The objective will be to control the attitude of the midpoint $x=0$ of the beam. At $x=0$ the slope of any antisymmetric mode $w_m(x)$ will be denoted w_{m0}'. The actuator and the sensor are placed at $x=0$; therefore, $w_{ma}' = w_{ms}' = w_{m0}'$. Various parameters of the free beam are chosen to be

$$2\ell = 200.0 \text{ m}; \ \rho_b = 0.0215 \text{ kg/m}; \ EI = 6.5 \text{ N.m}^2;$$
$$\zeta_m = 0.005, \ m = 1, \ldots, \infty, \qquad (50)$$

where ρ_b is the mass per unit length and EI is the bending rigidity of the beam. The lowest frequency of the beam is $\omega_1 = 0.02681$ rad/s. It is instructive to compare the frequency ω_1 with the rigid mode frequency $\omega_0 = 0.000264$ rad/s in Eq. (37).

Regarding the internal disturbance due to the actuator in Eq. (38d), the external disturbance $e(t)$ in Eq. (38c), and the constant disturbance considered in Eq. (16), we choose the following parameters

$$\sigma_e = 0.1 \text{ N.m}, \ \tau = 0.2 \text{ s}, \ V_a = 0.0002 \text{ N}^2.\text{m}^2/\text{s},$$
$$\zeta_a = 0.7, \ \sigma_0 = 0.1 \text{ N.m} \qquad (51)$$

The constant disturbance, denoted by the symbol σ_e in Eq. (16), is denoted σ_0 in Eq. (51). The bandwidth of the exponentially correlated noise $e(t)$ depends on how much of its power we wish to include in the model. If we retain $(1-\epsilon)$ fraction of the power, then the cutoff frequency ω_c is given by $\omega_c\tau = \tan(1-\epsilon)\pi/2$. For example, for $\tau = 0.2$ s and $\epsilon = 0.05$, ω_c and ω_{60} of the free beam are

$$\omega_c = 63.531 \text{ rad/s}, \qquad \omega_{60} = 62.295 \text{ rad/s},$$

suggesting that by considering 60 (antisymmetric) modes, 95% power of $e(t)$ is accounted for. We further note that the very high frequency modes of any space vehicle are spurious anyway and, as such, it is reasonable to ignore them. Consequently, in this numerical work the highest mode considered will be $m = 60$.

Modal Cost Analysis

In this subsection the control torque $u(t)$ in Eq. (38d) is zero. Moreover, since the actuator and the sensor dynamics are treated analogously, the latter will not be illustrated. Let $P_a(\omega)$ denote the power spectral density of the disturbance $u_a(t)$ in Eq. (38d). Then,

$$P_a(\omega) = V_a\omega_a^4/\{(-\omega^2 + \omega_a^2)^2 + (2\zeta_a\omega_a\omega)^2\} \qquad (52)$$

Since the three uncorrelated disturbances, u_a, e, and σ_0, are present simultaneously, Eqs. (11), (15), (16), (32), and (33) lead to

$$E(\eta_m^2)_\infty = w_{m0}'^2 P(\omega_m)/4\zeta_m\omega_m^3 + w_{m0}'^2\sigma_0^2/\omega_m^4,$$
$$E(\theta_m^2)_\infty = w_{m0}'^2 E(\eta_m^2)_\infty$$
$$E(\dot\eta_m^2)_\infty = w_{m0}'^2 P(\omega_m)/4\zeta_m\omega_m,$$
$$E(\dot\theta_m^2)_\infty = w_{m0}'^4 P(\omega_m)/4\zeta_m\omega_m \qquad (53)$$

where $P(\omega_m) \triangleq P_e(\omega_m) + P_a(\omega_m)$. The four modal indices in Eqs. (53) are shown in Fig. 3 where the effect of the break

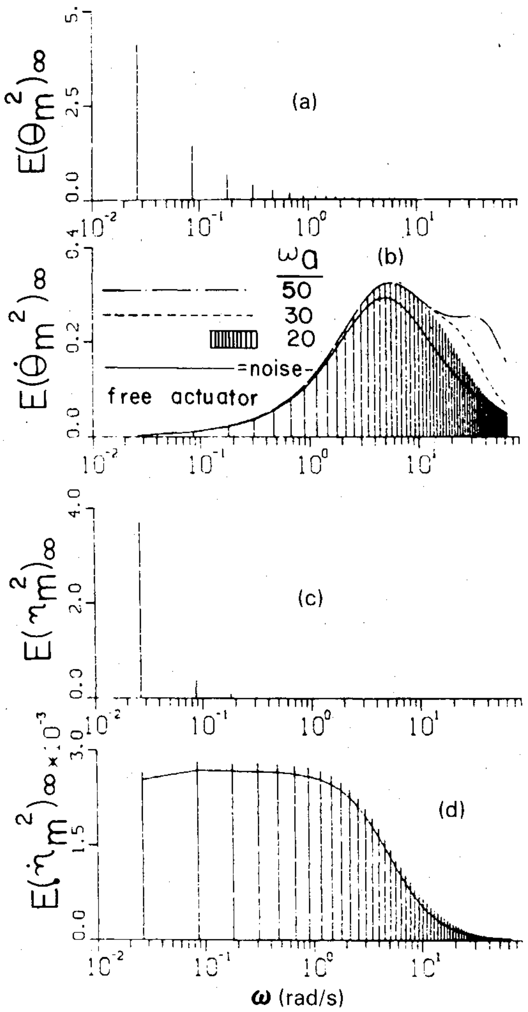

Fig. 3 The four modal indices: a) attitude; b) attitude rate; c) modal coordinates; d) modal coordinate rates.

frequency ω_a of the actuator on the modal excitation is also portrayed.

To interpret Fig. 3, recall that w'_{m0} is proportional to $\omega_m^{1/2}$; the attitude $\theta(t)$ still remains finite because $\eta_m(t)$ never increases monotonically with m. Substantiating this remark, Fig. 3a displays a rapid reduction of $E(\theta_m^2)_\infty$ vs ω. Figure 3b portrays a variation of $E(\dot{\theta}_m^2)_\infty$ for $\omega_a = 50$, 30, and 20 rad/s, and for the disturbance $e(t)$ alone. We see that as the break frequency ω_a of the actuator increases, $E(\dot{\theta}_m^2)_\infty$ for higher m's increases. This suggests the necessity of a moderate ω_a. Since for $\omega_a = 20$ rad/s the $E(\dot{\theta}_m^2)_\infty$ due to the actuator noise is not very significant, we select this value for further computations. Also, Fig. 3b conveys the benefits of modeling the disturbances with their bandwidths in that after an initial increase with m the $E(\dot{\theta}_m^2)_\infty$ does reduce for higher m's.

Figures 3c and 3d show $E(\eta_m^2)_\infty$ and $E(\dot{\eta}_m^2)_\infty$ vs ω_m. Note that the steady-state kinetic energy, $\Sigma E(\dot{\eta}_m^2)_\infty$, in Fig. 3d is the same as the steady-state deformational energy, $\Sigma E(\omega_m^2 \eta_m^2)_\infty$. Figures 3c and 3d state that although the beam deformation $w(x,t)$, defined as

$$w(x,t) \triangleq x\eta_0(t) + \sum w_m(x)\eta_m(t), \tag{54}$$

consists primarily of the first few modes, the deformational energy or the kinetic energy is distributed among a much larger number of modes. Also, note that the energy of a mode, $E(\dot{\eta}_m^2)_\infty$, is proportional to the power spectral density $P(\omega_m)$ at the modal frequency ω_m.

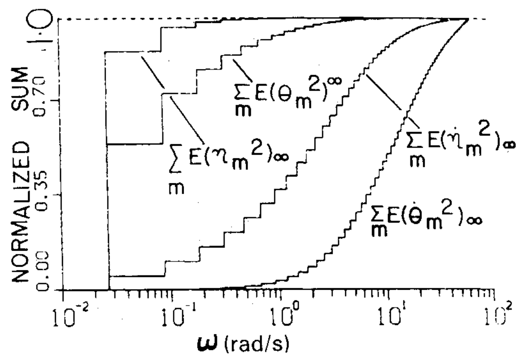

Fig. 4 The four normalized sums.

It is useful to know how the sums

$$\sum_{m=1}^{S} E\left(\theta_m^2, \dot{\theta}_m^2, \eta_m^2, \dot{\eta}_m^2\right)_\infty, S \leq 60 \tag{55}$$

grow as S increases. These sums, shown in Fig. 4, are normalized to unity for $S = 60$. We infer from Figs. 3 and 4 that in the present example, shape control of the beam requires fewest modes, the attitude control of the midpoint $x = 0$ requires a larger number of modes, control of the kinetic or the deformational energy requires a still larger number, and the attitude rate control of the midpoint requires the largest number of modes to compose a finite model of a specified accuracy.

While Figs. 3 and 4 depict modal information about the beam, Fig. 5 displays the spatial variation of $E[w^2(x,t)]_\infty^{1/2}$ and $E[\dot{w}^2(x,t)]_\infty^{1/2}$ of the beam itself. Only the right half of the beam is displayed, the left half being antisymmetric to it. Clearly, the deformed shape is almost entirely determined by the first few antisymmetric modes, $w_m(x)$. The deformational energy density in Fig. 5b is virtually constant over the entire beam except in a narrow region near the midpoint where the disturbances are active, and near $x = -\ell, \ell$ where the ends are free. The constant disturbance σ_0 and the rigid mode $\eta_0(t)$ are not considered in Fig. 5.

With the aid of Fig. 3 a finite number of modes can now be selected. As stated earlier, our basic objective is to control the attitude $\theta(t)$ of the beam; the objectives of controlling the attitude rate and the kinetic and strain energies in Eq. (42) have been included only to illustrate that the modal cost analysis is useful for any performance index. Moreover, since only attitude measurements are available, the output feedback scheme will be unable to control the attitude rate or energy whatever may be the weighting scalars β and γ in Eq. (42). Consequently, we may reasonably select $\beta = 1$ and $\gamma = 10$ for

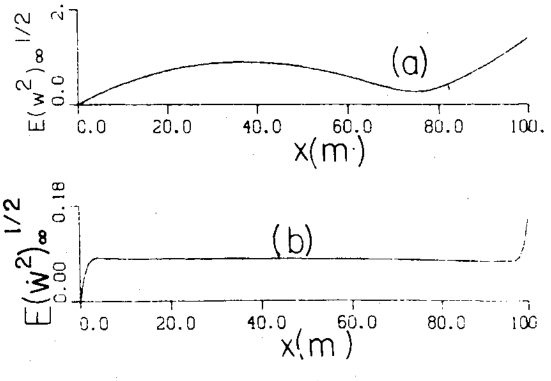

Fig. 5 Steady state RMS shape and velocity of the beam.

which the mode sequence is

$$\mathscr{S}(N) = 1,2,3,4,5,16,17,15,18,14,19,13,20,12,21,22,$$
$$11,6,23,10, \vdots\ 24,9,25,7,8,26,27,\ldots \tag{56}$$

For $N=20$, that is, up to the mode $m=10$ in the sequence (56), the normalized $J(N)$ and the four sums corresponding to the modal indices of Sec. II are

$$J(20) = 0.6627, \sum E\left(\eta_m^2, \theta_m^2, \dot{\eta}_m^2, \dot{\theta}_m^2\right)_\infty$$
$$= (0.996, 0.950, 0.670, 0.400) \tag{57}$$

The maximum value of the sums in Eq. (57) is unity. From these sums we deduce that the shape of the beam is well contained in these modes, the attitude $\theta(t)$ and the kinetic energy are the next, and the attitude rate is the least well represented. The index $J(20)$ is somewhat low due to a low $\Sigma_{m\in\mathscr{S}(20)} E(\dot{\theta}_m^2)_\infty$ but this may be tolerable because $\Sigma_{m\in\mathscr{S}(20)} E(\theta_m^2)_\infty = 0.95$ which is considered to be satisfactory. The state space model (41) corresponding to $\mathscr{S}(20)$ is now constructed.

Performance of the Optimal Output Feedback Controller

The iterative procedure described in Sec. III for determining the optimal output feedback (OOFB) gain M is used here. In the application of such iterative algorithms the convergence is often a problem. However, since we are dealing with a single-input, single-output system, such difficulties are not encountered; see Fig. 6a. The number of iterations required increases as the control weighting scalar ρ decreases. Figure 6b shows that the gain M increases as the number of retained modes increases. We also observe that the difference between the OOFB and the minimum error excitation (MEE) gains reduces as N increases from 10 to 20. This suggests that for the problem under consideration, the better the fidelity of the model, the closer the MEE gain is to the OOFB gain.

Attention is now focused on the performances of the techniques MEE and OOFB as compared to that of an optimal state feedback (OSFB) approach. The following notations have been used in Fig. 7:

$$(J_\theta, J_{\dot{\theta}}, J_u) = E(\theta^2, \dot{\theta}^2, u^2)_\infty;\ ke = E\left(C\dot{\eta}_0^2 + \sum \dot{\eta}_m^2\right)_\infty \tag{58}$$

where these quantities have been displayed against the controller weighting scalar ρ. Recall that the four sums of the modal indices in (57) imply that J_θ in Fig. 7a is nearly the

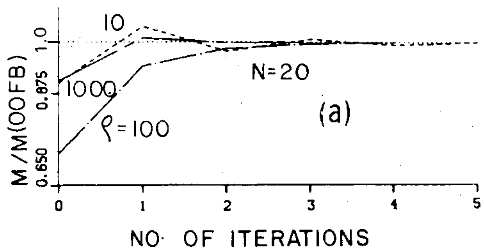

Fig. 6a Convergence of optimal output feedback gains.

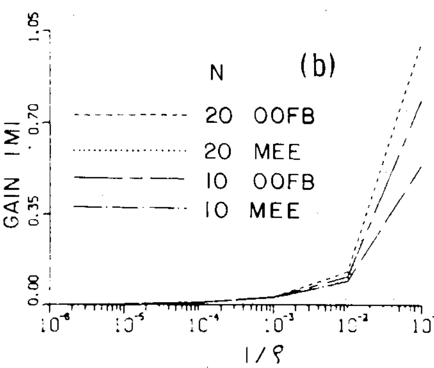

Fig. 6b Absolute values of controller gains.

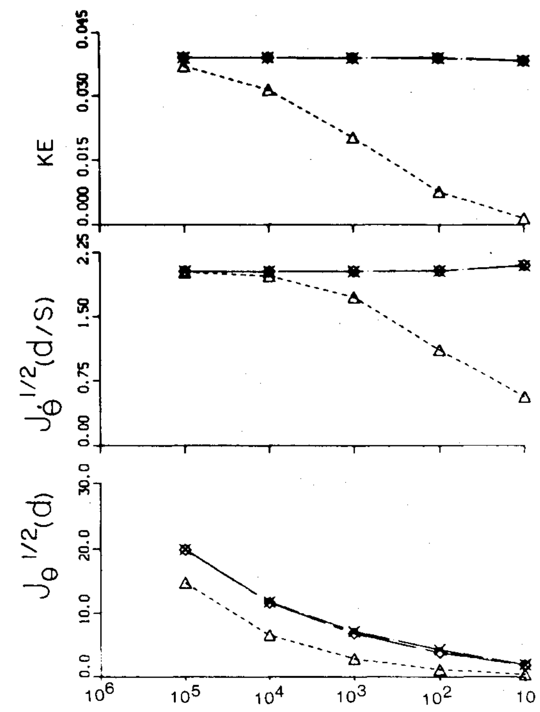

a)

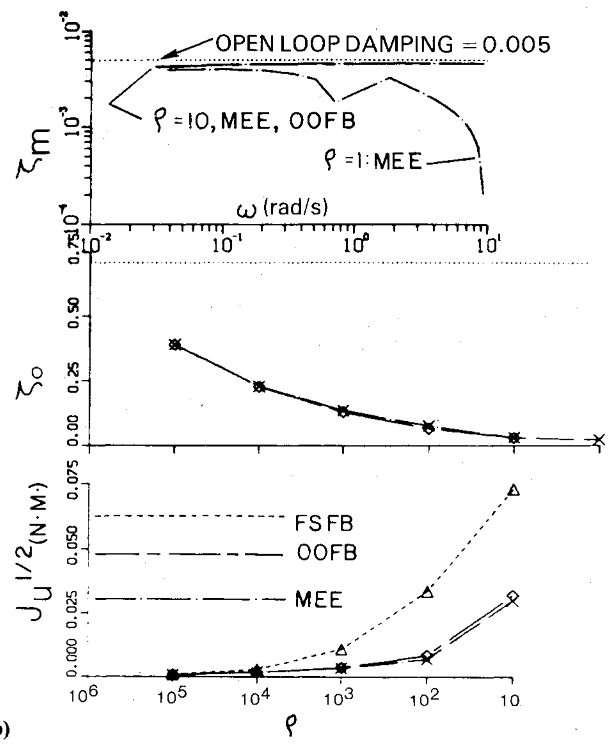

b)

Fig. 7 Comparison of performances of three controllers: a) attitude, attitude rate, and kinetic energy; b) control torque, "rigid" and elastic modal damping coefficients.

same as would be computed by letting the controller drive the untruncated model, unless the controller is driven too hard or the system is unstable. A similar statement cannot be made about the kinetic energy or the attitude rate. Returning to Fig. 7a we observe that the performance of MEE is practically the same as that of OOFB. Both perform remarkably well in controlling the attitude, a reduction from 20 to nearly 1.85 deg, because a position sensor is available. However, as expected, J_θ and ke remain practically unaffected. Figure 7b illustrates that both the control schemes seriously diminish the damping coefficient ζ_0 of the "rigid mode" in Eq. (38a). This, although a natural consequence of the control methodology adopted here, is unfortunate because such a reduction implies deterioration in the transient response of the spacecraft. Further, we observe that for $\rho \simeq 10$, both the feedback schemes reduce the modal viscous damping coefficient ζ_m, $m \in \mathscr{S}(20)$, from 0.005 to 0.004. One major difference between the two schemes was found for $\rho = 1$, for which the MEE reduced ζ_0 and ζ_m, $m \in \mathscr{S}(20)$, whereas the OOFB algorithm became unstable. Furthermore, although the performance index J, defined by Eq. (42), will be less for the OOFB than for the MEE, the OOFB is found to impose more control energy expenditure, J_u, than did the MEE. Also, note how minute the maximum control torque really is: nearly 0.025 N.m for the OOFB with $\rho = 10$. Finally, due to the assumption of the availability of all the state variables, the performance of the optimal state feedback is found always to be better than that of OOFB and MEE.

For completeness we mention that the Riccati and the Liapunov equations were solved by the programs composed by Laub[21] and Armstrong,[22] respectively, and that the computations were performed in double precision on the computer UNIVAC 1110.

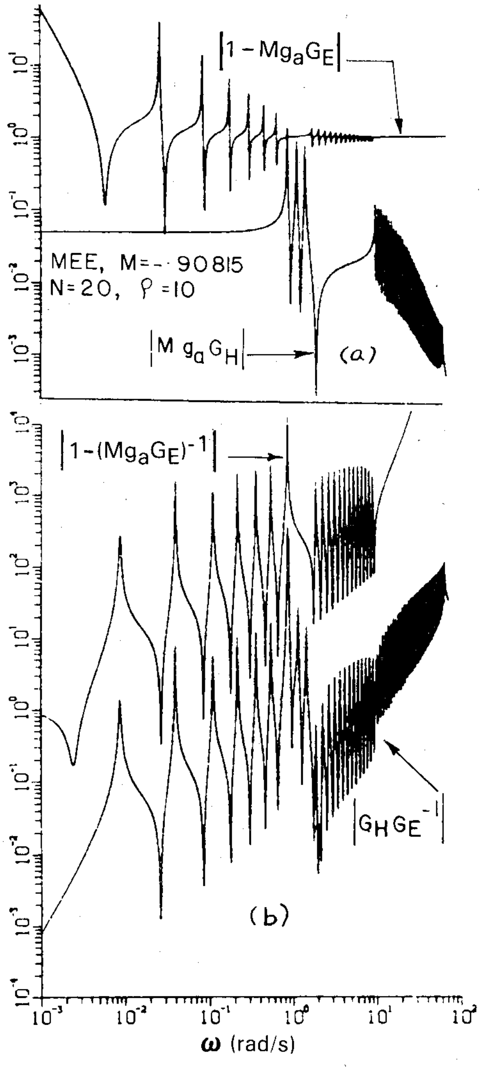

Fig. 8 Robustness inequalities as applied to truncated modes and output feedback controller: a) additive perturbation; b) multiplicative perturbation.

Table 1 Frequency and damping coefficient of mode 25 vs controller gain M

M	ω_{25}, rad/s	ζ_{25}
-0.90815	10.945	0.00459
-1.50	10.948	0.00431
-5.0	10.962	0.00248
-7.5	10.972	0.00097
-8.5	10.976	0.00031

Truncated Modes and Stability of the Output Feedback Controller

Any instability due to the modes truncated from the sequence (56) after the mode $m = 10$ may be detected by using the robustness inequalities of Eq. (49). It turns out that the violation, if any, of the inequalities is visually clearer in the case of (49b) than in the case of (49a). Therefore, Fig. 8a shows the inequality (49b) for $N = 20$, $\rho = 10$, $M = -0.90815$ (MEE approach). The inequality is shown to be violated at two frequencies. It is disconcerting to observe that one of the causes of the violation is the mode 7, the 24th mode in the sequence (56) and considered to be unimportant from the viewpoint of performance. By reducing the gain to $M = -0.09254$ for $\rho = 100$, however, the violations disappear as shown in Fig. 8b, which illustrates the multiplicative inequality, Eq. (49a). In our work we found that the violation results from the two inequalities concur. Therefore, to conserve space two additional plots portraying (49a) for $\rho = 10$ and (49b) for $\rho = 100$ will not be presented.

Sandell[23] notes that the inequalities of Eq. (49) are only sufficient conditions of stability, and not necessary. Consequently, it is mandatory to check if the violations detected in Fig.8a imply an actual instability. This can be accomplished by determining the eigenvalues of an enlarged state space model which encompasses the truncated modes $m = 24, 9, 25, 7, 8$, from the sequence (56). The frequency and the damping coefficient associated with the highest eigenvalue of the corresponding closed-loop state matrix for various values of the controller gain M are recorded in Table 1. This highest eigenvalue corresponds to the mode 25 which was found to be the least damped mode. Surprisingly, until $M = -8.5$ an instability was *not* found, although the damping coefficient ζ_{25} dropped from the open-loop value 0.005 to 0.0003. At $M = -9.0$, however this mode became unstable, the closed-loop eigenvalue being $+0.000327 \pm j10.977$. We are thus led to the conclusion that the robustness inequalities of Eq. (49) are not adequate to detect instability due to the truncated modes.

VI. Concluding Remarks

The theoretical developments in the preceding sections were concerned with the stochastic dynamics and control of a flexible spacecraft whose attitude motion about at least one axis can be decoupled from the motion about the remaining two axes and from the translational motion. The analysis was subsequently illustrated by applying it to a free beam. These efforts may be summarized as follows:

1) The open-loop modal cost analysis has been extended to embrace disturbances having arbitrary power spectral densities, and sensors having arbitrary response spectral densities. This is accomplished with the aid of residue calculus. This result is useful in model order reduction, as it can account for

finite bandwidths of disturbances and sensors.

2) The importance of a mode for the shape or attitude control is inversely proportional to (modal frequency),^{3} whereas for the energy or attitude rate control it is inversely proportional to the modal frequency. Clearly, for a specified accuracy in the model, the former control problem requires fewer modes and the latter requires a greater number of modes.

3) For the beam problem, the minimum error excitation technique of designing a suboptimal output feedback controller appears to yield results as good as those of an optimal output feedback controller. This is beneficial in that the former imposes only linear computations, whereas the latter entails nonlinear optimization problems.

4) In the present study, the minimum error excitation technique consumes less control energy than does the optimal output feedback. Benefits in terms of energy savings in space are evident.

5) Truncated modes can be represented as an additive or a multiplicative perturbation in the nominal transfer function of a spacecraft. However, utility of this representation to detect an instability due to the truncated modes is limited because the associated robustness inequalities not only confine controller gains to a narrow range but also label a wrong mode as the cause of instability.

Remarks 3, 4, and 5 are believed to be valid in general because they were found to be true for a gyroscopic flexible spacecraft using four sensors and two actuators and having the attitude motion about two axes coupled; see Ref. 3.

Acknowledgments

We acknowledge the perceptive discussions and encouragement of Dr. Robert C. Ried, Head of Aerothermodynamics Section, NASA Johnson Space Center, Houston, Tx. at various stages of our endeavors. It is our pleasure to thank Mr. R. Rosencranz and Ms. Jo Anne Henderson of Computing Center for their help in computational labor. Also, we are indebted to the National Research Council for financial support. Finally, with much pleasure we thank the reviewers of this paper for critical reviews.

References

[1] Hughes, P. C. and Skelton, R. E., "Modal Truncation for Flexible Spacecraft," *Journal of Guidance, Control, and Dynamics* Vol. 4, May-June 1981, pp. 291-297.

[2] Skelton, R. E. and Hughes, P. C., "Flexible Spacecraft Model Reduction and Control Design by Modal Cost Analysis," *Proceedings of the Second VPI&SU/AIAA Symposium on Dynamics and Control of Large Flexible Spacecraft*, Blacksburg, Va., L. Meirovitch, ed., June 1979, pp. 641-660.

[3] Hablani, H. B., "Dynamics and Control of a Deformable Gyrostat, Utilizing Continuum Vehicle Modes," *Journal of Guidance, Control, and Dynamics*, Vol. 6, Nov.-Dec. 1983, pp. 499-510.

[4] Ashkenazi, A., and Bryson, A. E., "Control Logic for Parameter Insensitivity and Disturbance Attenuation," *Journal of Guidance, Control, and Dynamics*, Vol. 5, No. 4, July-Aug. 1982, pp. 383-388.

[5] Pearson, R. K. and Johnson, T. L., "An Alternative View of the Optimal Output Feedback Compensation Problem," *Proceedings of the Third VPI&SU/AIAA Symposium on Dynamics and Control of Large Flexible Spacecraft*, Blacksburg, Va., L. Meirovitch, ed., June 1981, pp. 79-88.

[6] Lin, J. G., Hegg, D. R., Lin, Y. H. and Keat, J. E., "Output Feedback Control of Large Space Structures: An Investigation of Four Design Methods," *Proceedings of the Second VPI&SU/AIAA Symposium on Dynamics and Control of Large Flexible Spacecraft*, Blacksburg, Va., L. Meirovitch, ed., June 1979, pp. 1-18.

[7] Kosut, R. L., "Suboptimal Control of Linear Time Invariant Systems Subject to Control Structure Constraints," *IEEE Transactions on Automatic Control*, Vol. AC-15, Oct. 1970, pp. 557-563.

[8] Hegg, D. R., "Extensions of Suboptimal Output Feedback Control with Application to Large Space Structures," *Journal of Guidance, Control, and Dynamics*, Vol. 4, Nov.-Dec. 1981, pp. 637-641.

[9] Doyle, J. C. and Stein, G., "Multivariable Feedback Design: Concepts for a Classical/Modern Synthesis," *IEEE Transactions on Automatic Control*, Vol. AC-26, No. 1, Feb. 1981, pp. 4-16.

[10] Nuzman, D. W. and Sandell, N. R., "An Inequality Arising in Robustness Analysis of Multivariable Systems," *IEEE Transactions on Automatic Control*, Vol. AC-24, No. 3, June 1979, pp. 492-493.

[11] Kosut, R. L., Salzwedel, H., and Emami-Naeini, "Robust Control of Flexible Spacecraft," *Journal of Guidance, Control and Dynamics*, Vol. 6, March-April 1983, pp. 104-111.

[12] Hughes, P. C., "Passive Dissipation of Energy in Large Space Structures," *Journal of Guidance, Control, and Dynamics*, Vol. 3, July-Aug. 1980, pp. 380-382.

[13] Crandall, S. H. and Wittig, L. E., "Chladni's Patterns for Random Vibration of a Plate," *Proceedings of a Symposium on Dynamic Response of Structures*, Stanford University, Stanford, Calif., G. Herrmann and N. Perrone, eds., June 1971, pp. 55-71.

[14] Elishakoff, I., Van Zanten, A. T. and Crandall, S. H., "Wide-Band Random Axisymmetric Vibration of Cylindrical Shells," *Journal of Applied Mechanics*, Vol. 46, June 1979, pp. 417-422.

[15] Kwakernaak, H. and Sivan, R., *Linear Optimal Control Systems*, Wiley-Interscience, New York, 1972.

[16] Hildebrand, F. B., *Advanced Calculus for Applications*, 2nd ed, Prentice Hall, Englewood Cliffs, N.J., 1976, pp. 539-621.

[17] Bendat, J. S. and Piersol, A. G., *Engineering Applications of Correlation and Spectral Analysis*, John Wiley and Sons, New York, 1980, pp. 115-116.

[18] Skudryzk, E., *Simple and Complex Vibratory Systems*, Pennsylvania State University Press, University Park, Pa., 1968, pp. 320-345.

[19] Wertz, J. R., ed., *Spacecraft Attitude Determination and Control*, D. Reidel Publishing Company, Boston, 1978, Chapters 6, 7.

[20] Hablani, H. B., "Synthesis of a modern/classical controller for Large Space Structures," Paper No. 82-1613, *Proceedings of AIAA Guidance and Control Conference*, San Diego, Calif., Aug. 1982, pp. 597-610.

[21] Laub, A. J., *A Schur Method for Solving Algebraic Riccati Equations*, LIDS-R-859, Massachusetts Institute of Technology, Cambridge, Mass., Oct. 1978.

[22] Armstrong, E. S., *ORACLS—A System for Linear-Quadratic-Gaussian Control Law Design*, NASA Technical Paper 1106, Langley Research Center, Hampton Va., 1972.

[23] Sandell, N. R., "Robust Stability of Multivariable Feedback Systems," *16th Annual Allerton Conference on Communications, Control and Computing*, Monticello, Ill., Oct. 1978, pp. 471-479.